Time-Delayed Positive Velocity Feedback Control Design for Active Control of Structures

Phailaung Phohomsiri[1]; Firdaus E. Udwadia[2]; and Hubertus F. von Bremen[3]

Abstract: In this paper we present and propose a design methodology that uses intentional time delays for the active control of structures. We use here positive velocity-feedback, time-delayed control and show that its performance is, in general, superior to the previously developed methodology of using time delayed, negative velocity-feedback control. A detailed study carried out in this paper of the nonsystem poles and their interaction with the system poles reveals the reasons for this. Analytical results related to performance and stability of the new method are presented. We apply the time delayed positive velocity feedback active control methodology to a multidegree-of-freedom system subjected to the S00E component of ground acceleration recorded during the El Centro 1940 earthquake. The excellent behavior in terms of stability, performance, and control efficiency that is demonstrated by our time-delayed control design as well as its facile implementation makes it attractive for earthquake hazard mitigation in a practical sense.

DOI: 10.1061/(ASCE)0733-9399(2006)132:6(690)

CE Database subject headings: Active control; Earthquake engineering; Stability; Delay time; Velocity; Structural control.

Introduction

It is known that unavoidable time delays in the active control of large civil engineering structures arise due to sensing vibrational data, filtering these data, calculating control forces, and applying the computed control forces. Nonsynchronized control as a result of time delays in the control loop may cause a deterioration of performance and stability of structural control. That is why numerous scientists and engineers (Satche 1949; Choksy 1962; Marshall 1974; Abdel-Rohman 1985; 1987; Sain et al. 1992; Agrawal et al. 1993; Udwadia and Kumar 1994a,b; Agrawal and Yang 1997, 2000) have attempted to eliminate and/or reduce the effects of time delays in the feedback control loop. However, most of the techniques developed to date have been based on the restriction that the time delays need to be relatively small, compared to the natural periods of vibration of the system and often, in large complex structures, time delays that are a significant proportion of a natural frequency of vibration of the structure can, and do, arise (Kobori et al. 1991; Koike et al. 1994). It has been known for some time that the introduction of small time delays in the feedback control loop can make noncollocated velocity control (which would otherwise be unstable) stable (Udwadia 1991, 1992; Udwadia and Kumar 1994a,b; von Bremen and Udwadia 2000; 2001; Udwadia et al. 2003). However, only recently has attention been focused on the use of control methodologies that intentionally introduce large time delays (Udwadia et al. 2005) in the feedback control loop for active structural control. They (Udwadia et al. 2005) make use of time-delayed, negative velocity feedback for structural control and demonstrate its usefulness. Using intentional time delays in the vicinity of the natural period of the system, they show that performance and stability of time-delayed velocity feedback control are satisfactory.

While utilizing the same basic design principles as in Udwadia et al. (2005), in this paper we use time-delayed, positive velocity feedback to control structures and use intentional time delays in the vicinity of half the natural period of vibration. Here again, conventional wisdom would proscribe such control since positive velocity feedback is known to be unstable; however we show that the introduction of a suitable time delay not only renders it stable, but also bestows upon it improved performance characteristics as well as improved control efficiency compared to time-delayed negative velocity feedback.

The structure of this paper is as follows. We first study the behavior of the so-called system poles. Since the time delayed system is infinite dimensional, we then take up the issue of this infinite dimensionality, and this leads us to the so-called nonsystem poles. We obtain formulae for their locations, provide analytical results related to their root loci, and go on to demonstrate the interaction between the system poles and the nonsystem poles. In the next section, we provide stability of time delayed positive feedback control for varying values of the time delay and the control gain. Subsequently, we present two applications of our control design methodology, and compare our results with those obtained earlier (Udwadia et al. 2005) using time-delayed negative velocity feedback, and negative velocity feedback with no time delay. We demonstrate the superiority of time-delayed positive velocity feedback using large, intentional time delays for a single degree of freedom (SDOF) system subjected to a synthetically generated base acceleration. We further show how

[1]Postdoctoral Fellow, Dept. of Aerospace and Mechanical Engineering, Univ. of Southern California, Los Angeles, CA 90089.

[2]Professor, Dept. of Civil Engineering, Aerospace and Mechanical Engineering, Mathematics, and Information and Operations Management, Univ. of Southern California, 430K Olin Hall, Los Angeles, CA 90089-1453 (corresponding author). E-mail: fudwadia@usc.edu

[3]Assistant Professor, Dept. of Mathematics, Univ. of Southern California, Los Angeles, CA 90089.

Note. Associate Editor: Raimondo Betti. Discussion open until November 1, 2006. Separate discussions must be submitted for individual papers. To extend the closing date by one month, a written request must be filed with the ASCE Managing Editor. The manuscript for this paper was submitted for review and possible publication on October 11, 2004; approved on July 14, 2005. This paper is part of the ***Journal of Engineering Mechanics***, Vol. 132, No. 6, June 1, 2006. ©ASCE, ISSN 0733-9399/2006/6-690–703/$25.00.

to apply our design procedure to a structure modeled as a 3 degree-of-freedom system subjected to the S00E component of ground acceleration recorded in the El Centro Earthquake of 1940. This leads to a time-delayed, noncollocated, distributed, control strategy. Our numerical results show that time delayed positive velocity feedback with intentional time delays can be designed to be superior in terms of stability, performance, and control force efficiency to time-delayed negative velocity feedback control. In fact, our example shows it could be made very comparable in its performance and control efficiency to (the usual) negative velocity feedback with no time delay. Then, we attempt to explain the physics of time delayed control that utilizes large, intentional time delays, in view of the light shed by the analytical results developed in previous sections. Finally, we state our conclusions.

Behavior of System Poles

Consider a SDOF system subjected to external excitation with time-delayed positive velocity feedback

$$\ddot{x} + 2\omega_n\zeta_n\dot{x} + \omega_n^2 x = g_v\dot{x}(t - T_d) + f(t) \tag{1}$$

where ω_n and ζ_n=natural frequency and the damping ratio of the uncontrolled system, respectively. The first term on the right hand side of Eq. (1) represents positive velocity feedback, which is delayed by a time $T_d > 0$, with a gain of $g_v > 0$, and $f(t)$ is the external excitation which is a function of time t.

The characteristic equation of the system, obtained by taking Laplace transforms of the Eq. (1), is given by

$$s^2 + 2\omega_n\zeta_n s + \omega_n^2 - g_v s\exp(-sT_d) = 0. \tag{2}$$

When the gain g_v is zero, the complex conjugate poles of the system, which are also the zeros of Eq. (2), are given by

$$s_{1,\bar{1}} = -\omega_n\zeta_n \pm i\omega_n\sqrt{1-\zeta_n^2} \tag{3}$$

These zeros correspond to the poles of the uncontrolled system. As the gain g_v is gradually increased, the zeros of Eq. (2) which start from $s_{1,\bar{1}}$ will change. The poles of the system that begin from $s_{1,\bar{1}}$ (when $g_v = 0^+$) and change as g_v is gradually increased will be called the "system poles." These system poles in fact are functions of both the time delay, T_d, and the gain, g_v. They can be expressed, similar to Eq. (3), as

$$s_{1,\bar{1}}(T_d, g_v; \omega_n, \zeta_n) = -\tilde{\omega}_n\tilde{\zeta}_n \pm i\tilde{\omega}_n\sqrt{1-\tilde{\zeta}_n^2} \tag{4}$$

where $\tilde{\omega}_n(T_d, g_v)$ and $\tilde{\zeta}_n(T_d, g_v)$=equivalent natural frequency of vibration and the equivalent damping factor, respectively. These are obtained from the relations

$$\tilde{\zeta}_n(T_d, g_v) = \frac{\delta}{\sqrt{1+\delta^2}} \tag{5}$$

and

$$\tilde{\omega}_n(T_d, g_v) = \frac{\mathrm{Im}[s_1(T_d, g_v)]}{\sqrt{1-\tilde{\zeta}_n^2}} \tag{6}$$

where

$$\delta = -\frac{\mathrm{Re}[s_1(T_d, g_v)]}{\mathrm{Im}[s_1(T_d, g_v)]} \tag{7}$$

Let us next divide Eq. (2) by ω_n^2 and use the normalized quantities $\tilde{s} = s/\omega_n$

$$\tau = \frac{T_d}{T_n} = \frac{\omega_n T_d}{2\pi}$$

and

$$\gamma_v = \frac{g_v}{\omega_n} > 0$$

(positive feedback) to get

$$\tilde{s}^2 + 2\zeta_n\tilde{s} + 1 - \gamma_v\tilde{s}\exp(-2\pi\tau\tilde{s}) = 0 \tag{8}$$

which is independent of ω_n. Similarly, we divide Eq. (4) by ω_n to obtain

$$\tilde{s}_{1,\bar{1}}(\tau, \gamma_v; \zeta_n) = -\tilde{\zeta}_n r \pm ir\sqrt{1-\tilde{\zeta}_n^2} \tag{9}$$

where $r = \tilde{\omega}_n/\omega_n$. As seen, the characteristic Eq. (8), and the poles, no longer explicitly depend on ω_n, which was the aim of our normalization.

From Eq. (8), we can find the root loci of the system poles by first starting from the location of the (conjugate pair of) system poles when $\gamma_v = 0$. Then, using the known values as initial guesses, as γ_v increases, the system poles (in the neighborhood of the initial guess) are computationally determined. Figs. 1(a–e) show the root loci of the system poles in the complex $\tilde{s}$ plane. Each curve in these figures is a root locus corresponding to a fixed value of the time delay τ. All the curves start at the location of the pole for the uncontrolled system ($\gamma_v = 0$). Along each root locus we also show the values of γ_v from 0 to 0.7 (highlighted in steps of 0.1 by increasingly larger dots). For purposes of design, root loci for five different values of ζ_n are shown. Since the roots arise in complex conjugate pairs, we show the root loci only in the upper half complex plane. It is seen from these figures that, as the gain increases, for small normalized time delays, τ, the root loci move steadily to the right half complex plane; for larger normalized time delays in the vicinity of $\tau = 0.5$, each root locus moves (initially) to the left. These latter loci provide a stable range of gain, around $\tau = 0.5$ because they start off almost horizontally and move left. As we further increase the dimensionless gain γ_v, however, the root loci begin to move right, and eventually they cross over into the right half complex plane. One observes a somewhat dramatic qualitative change in the root loci for $\tau = 0.5$ and 0.6 from bending downward to bending upward. This change, as we shall see in "Stability of Time Delayed Positive Velocity Feedback Control," is caused by a bifurcation created by the interaction of the system poles with the so-called nonsystem poles. Compared to similar figures for time-delayed, negative velocity feedback with $\tau \approx 1$ (Udwadia et al. 2005), time-delayed positive velocity feedback with $\tau \approx 0.5$ appears to be stable over a larger range of gains.

In the following, we give a closer analysis. Differentiating Eq. (8), we get

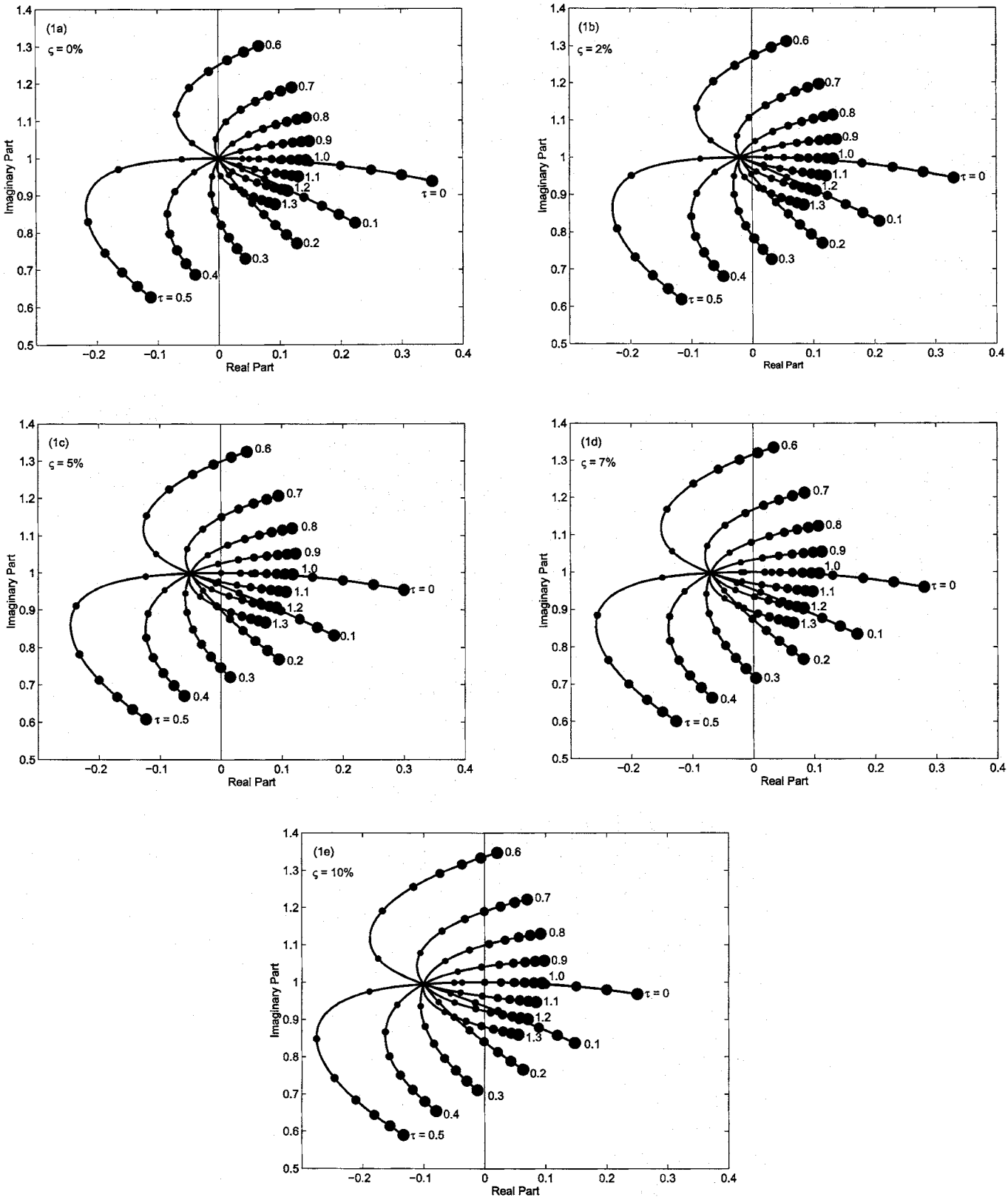

Fig. 1. Roots of Eq. (8) that start from roots of uncontrolled system in $\tilde{s}$ plane for different values of ζ_n, are system poles; their location is shown by curves. Numbers close to each curve show these root loci for different values of dimensionless time delay τ. Solid dots along each locus show values of dimensionless gain, γ_v (0.1, 0.2, 0.3, 0.4, 0.5, 0.6, and 0.7 by successively larger dots).

$$\frac{d\tilde{s}}{d\gamma_v} = \frac{\tilde{s}\exp(-2\pi\tau\tilde{s})}{2\tilde{s} + 2\zeta_n - \gamma_v \exp(-2\pi\tau\tilde{s}) + 2\pi\tau\gamma_v\tilde{s}\exp(-2\pi\tau\tilde{s})} \tag{10}$$

As $\gamma_v \to 0$, $\omega_n \approx \tilde{\omega}_n$ (or $r \approx 1$). Hence, $\tilde{s}_{1,\bar{1}}(\tau, \gamma_v \to 0; \zeta_n) \approx -\zeta_n \pm i\sqrt{1-\zeta_n^2}$. Considering the pole in the upper half complex plane $[\tilde{s}_{1,\bar{1}}(\tau, \gamma_v \to 0) \approx -\zeta_n + i\sqrt{1-\zeta_n^2}]$, we have

$$\lim_{\gamma_v \to 0} \frac{d\tilde{s}}{d\gamma_v} = \frac{\tilde{s}\exp(-2\pi\tau\tilde{s})}{2(\tilde{s} + \zeta_n)} = \frac{1}{2}\left(1 + \frac{i\zeta_n}{\sqrt{1-\zeta_n^2}}\right)\exp(2\pi\tau\zeta_n)\exp(-2\pi\tau i\sqrt{1-\zeta_n^2}) \tag{11}$$

For $\zeta_n \ll 1$, we get

$$\lim_{\gamma_v \to 0} \frac{d\tilde{s}}{d\gamma_v} = \frac{1}{2}\left(1 + \frac{i\zeta_n}{\sqrt{1-\zeta_n^2}}\right)\exp(2\pi\tau\zeta_n) \times \exp\left[-2\pi\tau i\left(1 - \frac{1}{2}\zeta_n^2 + \ldots\right)\right] = \frac{1}{2}\left(1 + \frac{i\zeta_n}{\sqrt{1-\zeta_n^2}}\right)\exp(2\pi\tau\zeta_n)\exp[-2\pi\tau i + iO(\tau\zeta_n^2)] \tag{12}$$

When $\tau = 0$ and $\tau = 1/2$, we obtain

$$\lim_{\gamma_v \to 0} \left.\frac{d\tilde{s}}{d\gamma_v}\right|_{\tau=0} = \lim_{\gamma_v \to 0}\left[\frac{d\,\mathrm{Re}(\tilde{s})}{d\gamma_v} + i\frac{d\,\mathrm{Im}(\tilde{s})}{d\gamma_v}\right]\Bigg|_{\tau=0} = \frac{1}{2}\left(1 + \frac{i\zeta_n}{\sqrt{1-\zeta_n^2}}\right) \tag{13}$$

and

$$\lim_{\gamma_v \to 0} \left.\frac{d\tilde{s}}{d\gamma_v}\right|_{\tau=1/2} = \lim_{\gamma_v \to 0}\left[\frac{d\,\mathrm{Re}(\tilde{s})}{d\gamma_v} + i\frac{d\,\mathrm{Im}(\tilde{s})}{d\gamma_v}\right]\Bigg|_{\tau=1/2} \approx -\frac{1}{2}\left(1 + \frac{i\zeta_n}{\sqrt{1-\zeta_n^2}}\right)\exp(\pi\zeta_n) \tag{14}$$

Eqs. (13) and (14) show that the root locus initially moves right when $\tau = 0$, while it moves left when $\tau = 1/2$. Nevertheless, the slopes of the rightward moving and leftward moving poles are the same (approximately ζ_n). This is also evident from Figs. 1(a–e).

Next, we find when the system first becomes unstable. We know that when root loci pass the imaginary axis ($\tilde{\zeta}_n = 0$), $\tilde{s}_{1,\bar{1}} = \pm ir$. Considering the system pole on the upper half of the complex $\tilde{s}$ plane, we have $\tilde{s}_1 = ir$. Thus, by Eq. (8) we have

$$[1 - r^2 - \gamma_v r\sin(2\pi\tau r)] + i[2\zeta_n r - \gamma_v r\cos(2\pi\tau r)] = 0 \tag{15}$$

The imaginary part of Eq. (15) gives

$$\gamma_v = \frac{2\zeta_n}{\cos(2\pi\tau r)} \tag{16}$$

Eq. (16) shows that for $\gamma_v > 0$ the system would be first unstable when $\tau = 0$ and the gain is about $2\zeta_n$. Also, the real part of Eq. (15) shows that $r = 1$, when $\tau = 0$.

We next show the relations between the equivalent damping factor (for $\zeta_n = 0.02$ and $\zeta_n = 0.05$) and the dimensionless gain, γ_v, with positive and negative velocity feedback. As shown in Figs. 2(a and b), with positive velocity feedback the equivalent damping factor for $\tau = 0.5$ is higher than that for $\tau = 0$, 0.4, and 0.6. Additionally, compared with negative velocity feedback (NVF) with $\tau = 1$, Fig. 2(a) shows that the equivalent damping factor for positive velocity feedback (PVF) with $\tau = 0.5$ has a higher value for gains $\gamma_v > 0.157$. And it also has a higher value, for $0 \leq \gamma_v \leq 0.44$, when compared with (direct) NVF without any time delay. The figure further shows that for a gain of 0.3, the values of the equivalent damping factor, for PVF with $\tau = 0.5$, for NVF with $\tau = 1$, and for NVF without any time delay, are about 0.26, 0.09, and 0.17, respectively. Clearly then, for control design purposes, one might suspect that it may be advantageous to use positive velocity feedback with $\tau \approx 0.5$ and gains in the neighborhood of 0.3 to achieve good performance, provided, of course, that control forces corresponding to these gains are practical to apply.

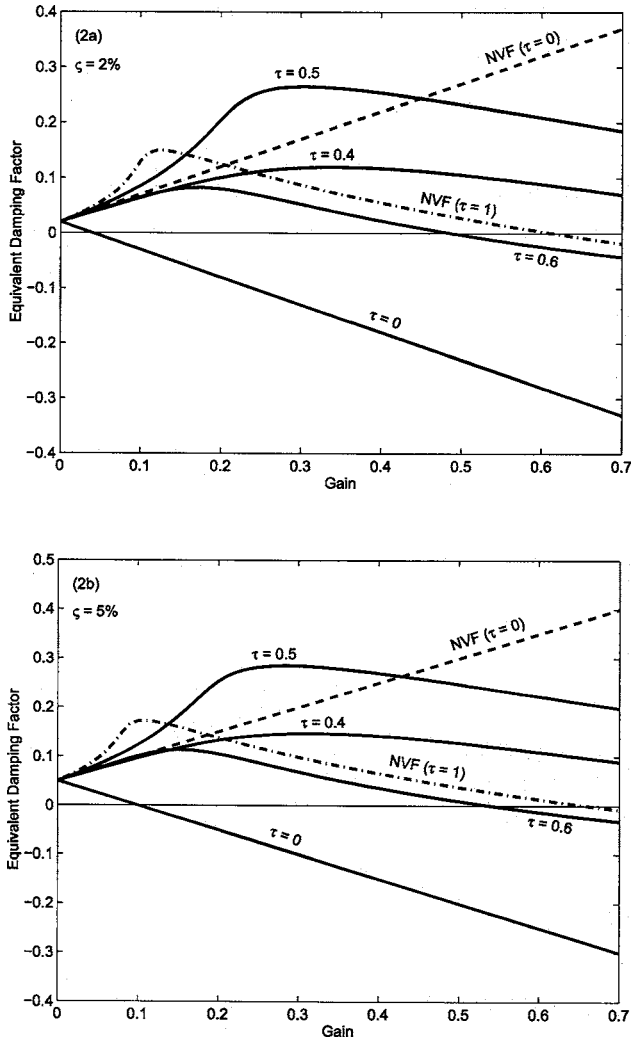

Fig. 2. Equivalent damping factor, $\tilde{\zeta}_n$, as function of modulus of gain, γ_v, for "system poles" for positive ($\tau = 0$, 0.4, 0.5, and 0.6) and negative ($\tau = 0$ and $\tau = 1$) velocity feedback system

In Figs. 3(a and b), we show that the normalized equivalent natural frequency $r = \tilde{\omega}_n(T_d, g_v)/\omega_n$ of vibration of the system is also affected by the presence of a time delay. We notice that for $\tau = 0.6$ with PVF the equivalent natural frequency is larger than ω_n ($r \geq 1$), but for $\tau = 0.4$ with PVF, for $\tau = 0.5$ with PVF, and for $\tau = 1$ with NVF, we find that $r \leq 1$. It is also noticed that for small gains the normalized equivalent natural frequency r remains

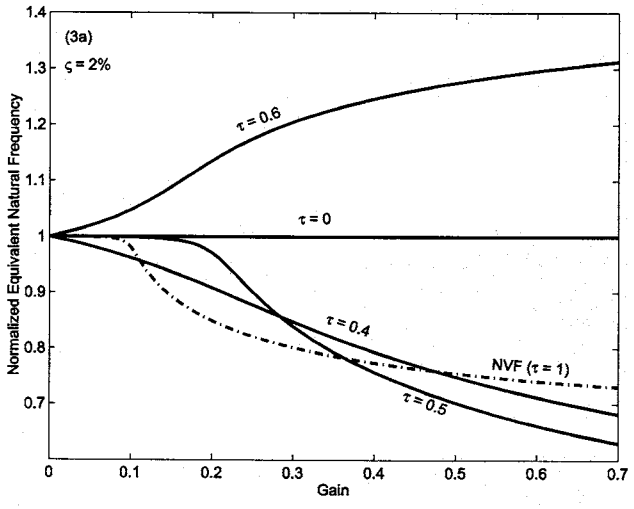

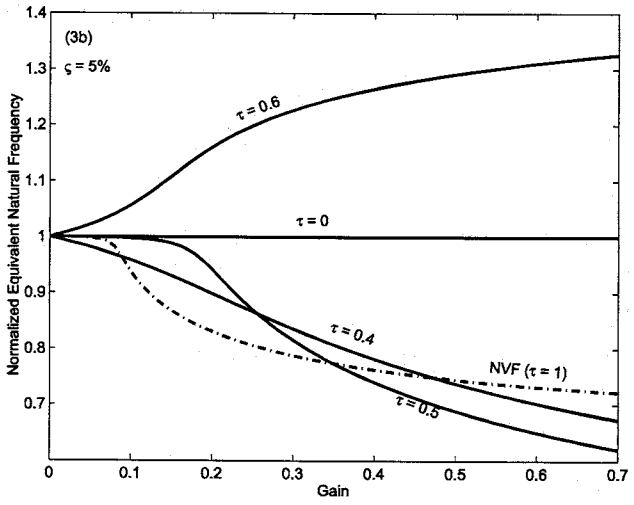

Fig. 3. Normalized equivalent natural frequency, $r=\tilde{\omega}_n/\omega_n$, as function of modulus of gain, γ_v, for system poles shown in Figs. 1(b and c)

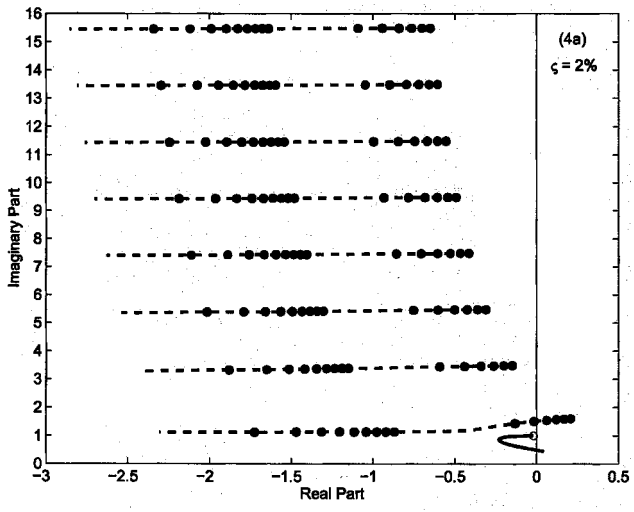

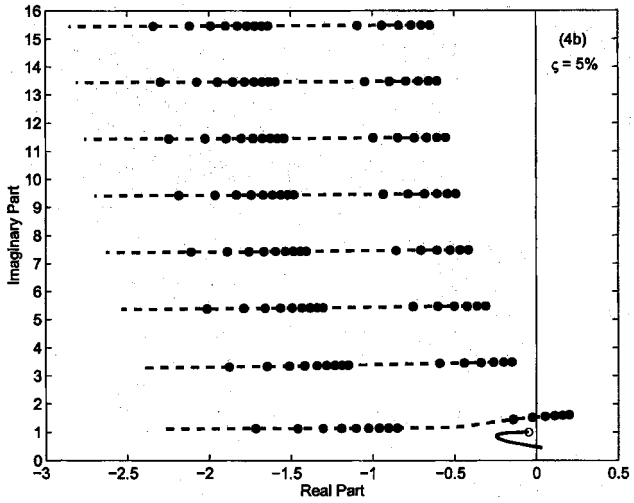

Fig. 4. Root loci of poles in complex $\tilde{s}$ plane for time delayed, positive velocity feedback with $\tau=0.5$ for: (a) $\zeta_n=2\%$ and (b) $\zeta_n=5\%$. Solid dots along each root locus represent locations of nonsystem poles at $\gamma_v=0.01$, 0.02, 0.03… 0.09, 0.5, 0.8, 1.1, 1.4, 1.7, and 2.0; leftmost point along each root locus is location of pole at $\gamma_v=0.001$. Solid line shows root locus of system pole starting with open circle where $\gamma_v=0$.

unchanged ($r\approx 1$) for both $\tau=1$ with NVF, and for $\tau=0.5$ with PVF; however, the range of gains over which $r\approx 1$ is greater for $\tau=0.5$. At higher gains the equivalent natural frequency $\tilde{\omega}_n$ for both $\tau=1$ with NVF and $\tau=0.5$ with PVF is less than ω_n, and the system's stiffness appears reduced.

Behavior of Nonsystem Poles

As pointed out in Udwadia et al. (2005), when the time delay is a considerable proportion of the natural frequency of vibration of the system, one cannot ignore the presence of the so-called nonsystem poles that are brought into existence by the presence of the time delay. This is because these poles can influence both the performance and the stability of the controlled system. In this section we study these nonsystem poles and their effect on the control design.

When $\gamma_v=0$ and $\zeta_n\geqslant 0$, the system has only the complex conjugate pair of system poles. We show this system pole by the open circle in the lower right corner of Fig. 4. As we increase the gain, an infinite number of poles, called "nonsystem poles" arise, entering (for $\gamma_v=0^+$) at the far left hand end of the complex $\tilde{s}$ plane (see Udwadia et al. 2005 for detailed analysis). As γ_v further increases, these nonsystem poles move right as shown in Fig. 4. The nonsystem poles are seen to move nearly horizontally in the complex $\tilde{s}$ plane and the vertical spacing between each root locus for PVF with $\tau=0.5$ is seen to be about a constant. A similar picture was developed for NVF with a time delay $\tau=1$ in Udwadia et al. (2005). However, a comparison of Fig. 4 with those obtained in Udwadia et al. (2005) shows that the spacing between the root loci for PVF with $\tau=0.5$ is roughly twice that reported in Udwadia et al. (2005). Moreover, unlike NVF with $\tau=1$, there are no nonsystem poles on the real axis, as we shall prove shortly.

We can now see the importance of the nonsystem poles in dictating the behavior of time delayed velocity feedback control. For $\zeta_n=0.02$ and $\tau=0.5$, Fig. 4(a) shows that the nonsystem pole that has the smallest ordinate is the first to cross into the right half complex $\tilde{s}$ plane; this happens when the dimensionless gain $\gamma_v\approx 0.8557$. On the other hand, from Fig. 1(b) we see that the

system pole for this value of gain remains in the left half complex plane and, in fact, crosses into the right half when the gain is increased to $\gamma_v \approx 1.5424$. A similar situation occurs for $\zeta_n = 0.05$ and $\tau = 0.5$ [see Figs. 4(b) and 1(c)]. Again, the nonsystem pole that first crosses over into the right half plane does so when $\gamma_v \approx 0.8903$; on the other hand, the system pole crosses the imaginary axis for a much larger value of gain, $\gamma_v \approx 1.6056$. We therefore see that it is the nonsystem poles that control the stability of the system. For $\zeta_n = 0.02$, the maximum gain that still keeps the time delayed system (with $\tau = 0.5$) stable is $\gamma_v \approx 0.8557$, whereas for $\zeta_n = 0.05$ the maximum gain that keeps the system stable is $\gamma_v \approx 0.8903$, and both these values of the gain arise from the behavior of the nonsystem poles.

In the following, we obtain some analytical results that will be useful for control design purposes. Starting with substituting the exponential terms obtained from Eq. (8) in Eq. (10), we get

$$\frac{d\tilde{s}}{d\gamma_v} = \frac{\tilde{s}}{\gamma_v} \frac{1}{2\pi\tau\tilde{s} + 1 - \dfrac{2\zeta_n\tilde{s} + 2}{\tilde{s}^2 + 2\zeta_n\tilde{s} + 1}} \tag{17}$$

Defining

$$\tilde{s} = R\exp[i(\pi - \varphi)] = -R\exp(-i\varphi) \tag{18}$$

where R=positive real number and φ=angle measured from the negative real axis in the clockwise direction, we obtain

$$\begin{aligned}
\frac{d\tilde{s}}{d\gamma_v} &\approx \frac{\tilde{s}}{\gamma_v}\left[\frac{1}{2\pi\tau\tilde{s} + 1 + O\left(\dfrac{\zeta_n}{R}\right)}\right] \\
&\approx \frac{1}{2\pi\tau\gamma_v}\left(\frac{1}{1 + \dfrac{1}{2\pi\tau\tilde{s}}}\right) \\
&\approx \frac{1}{2\pi\tau\gamma_v}\left[\frac{1}{1 - \dfrac{\exp(i\varphi)}{2\pi\tau R}}\right] \\
&= \frac{1}{2\pi\tau\gamma_v}\left[\frac{1 - \dfrac{\cos\varphi}{2\pi\tau R} + \dfrac{i\sin\varphi}{2\pi\tau R}}{1 - \dfrac{\cos\varphi}{\pi\tau R} + O\left(\dfrac{1}{R^2}\right)}\right]
\end{aligned} \tag{19}$$

for $R \gg 1$.

For a large time delay compared to the natural period of vibration of the system and $R \gg 1$, Eq. (19) can be reduced to

$$\begin{aligned}
\frac{d\tilde{s}}{d\gamma_v} &\approx \frac{1}{2\pi\gamma_v\tau} + O\left(\frac{1}{\gamma_v\tau^2 R}\right) + \frac{i}{4\pi^2\gamma_v\tau^2 R}\sin\varphi \\
&\approx \frac{1}{2\pi\gamma_v\tau} + iO\left(\frac{1}{\gamma_v\tau^2 R}\right)
\end{aligned} \tag{20}$$

It is seen that the rate of change of the real part of the nonsystem poles with respect to gain is inversely proportional to the product $\gamma_v\tau$. The rate of change of the imaginary part of the nonsystem poles is relatively much smaller when compared with that of the real part. This shows that, for small values of γ_v, the nonsystem poles travel swiftly right and relatively slowly upward in the complex $\tilde{s}$ plane, as evidenced from the root loci shown in Fig. 4. These statements are true when $R \gg 1$ and the time delays are large compared to the natural period of vibration of the system.

Substituting Eq. (18) in Eq. (8), we obtain

$$\begin{aligned}
&R\left[1 - \frac{2\zeta_n\exp(i\varphi)}{R} + \frac{\exp(i2\varphi)}{R^2}\right] \\
&\quad = -\gamma_v\exp(i\varphi)\exp(2\pi\tau R\cos\varphi)\exp(-i2\pi\tau R\sin\varphi)
\end{aligned} \tag{21}$$

Taking logarithms on both sides of Eq. (21), for $R \gg 1$, we get

$$\begin{aligned}
&\left[\ln R - \ln\gamma_v - \frac{2\zeta_n\cos\varphi}{R} + \frac{\cos 2\varphi}{R^2} - 2\pi\tau R\cos\varphi\right] \\
&\quad + i\left[-\frac{2\zeta_n\sin\varphi}{R} + \frac{\sin 2\varphi}{R^2} - \varphi + 2\pi\tau R\sin\varphi - (2n+1)\pi\right] = 0
\end{aligned}$$

$$n = 0, \pm 1, \pm 2, \ldots \tag{22}$$

When the root loci cross the imaginary axis ($\varphi = \pi/2$), for $R \gg 1$ the imaginary part of Eq. (22) gives

$$R \approx \frac{1}{\tau}\left(\frac{3}{4} + n\right) \quad n = 0,1,2,\ldots \tag{23}$$

Eq. (23) estimates the locations of the root loci of the nonsystem poles crossing the imaginary axis for time-delayed PVF and shows that the vertical spacing between each root locus where it crosses the imaginary axis is approximately proportional to $1/\tau$. We note that R in Eq. (23) is actually measured along the imaginary axis.

Similarly, the real part of Eq. (22), when $\varphi = \pi/2$ and $R \gg 1$, gives

$$\gamma_v \approx R\exp\left(-\frac{1}{R^2}\right) = \frac{1}{\tau}\left(\frac{3}{4} + n\right)\exp\left[-\frac{16\tau^2}{(3+4n)^2}\right] \quad n = 0,1,2,\ldots \tag{24}$$

Eq. (24) shows that the gain at which the nonsystem poles cross over into the right half complex plane is also approximately proportional to $1/\tau$.

When compared with numerically computed results, we find that relations (23) and (24) that we have obtained may be acceptable even when R is not large. For example, for $n=7$ we have $R=15.5$ and $\gamma_v = 15.4356$ as obtained by relations (23) and (24), while numerical computations give $R=15.5008$ and $\gamma_v = 15.4364$. Similarly, for $n=1$ relations (23) and (24) give $R=3.5$ and $\gamma_v = 3.2256$, while numerical computations give $R=3.5039$ and $\gamma_v = 3.2188$.

Since the vertical spacing between the nonsystem poles for time-delayed NVF is also proportional to $1/\tau$ (see Udwadia et al. 2005), we have the following observations: the gains at which the nonsystem poles cross the imaginary axis in the complex $\tilde{s}$ plane when using time delayed PVF with $\tau = 0.5$ are about twice those at which they cross the imaginary axis when using time-delayed NVF with $\tau = 1$. The spacing between the root loci of the nonsystem poles for PVF (with $\tau = 0.5$) is about double that for NVF (with $\tau = 1$). This points to the fact that when using PVF there is, in general, less interaction between the system and the nonsystem poles compared to NVF.

In the following, we will show that in the $\tilde{s}$ plane there is no root locus for PVF on the negative real axis.

Again, from Eq. (8), we can have

$$\gamma_v = \frac{\tilde{s}^2 + 2\zeta_n\tilde{s} + 1}{\tilde{s}\exp(-2\pi\tilde{s})} \tag{25}$$

On the negative real axis $\varphi = 0$, Eq. (18) gives $\tilde{s} = -R$. Thus, by Eq. (25) we require that for $\gamma_v > 0$

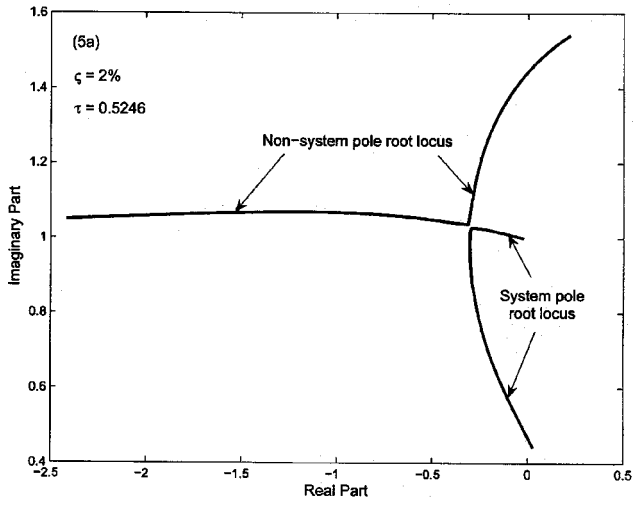

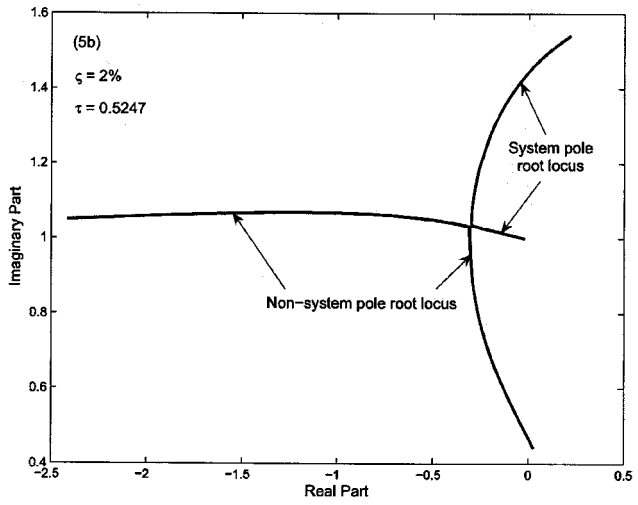

Fig. 5. Qualitative change (bifurcation) in root loci caused by interaction between root loci of system and nonsystem poles. For $\tau > \tau_b$ system pole "flips" upwards and equivalent natural frequency of time-delayed positive velocity feedback system increases.

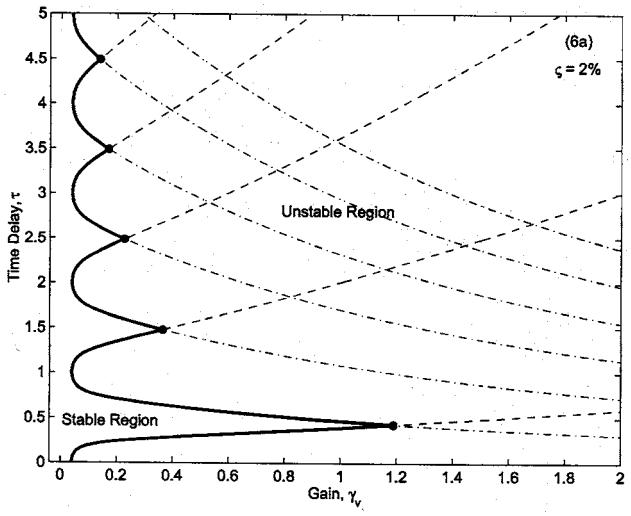

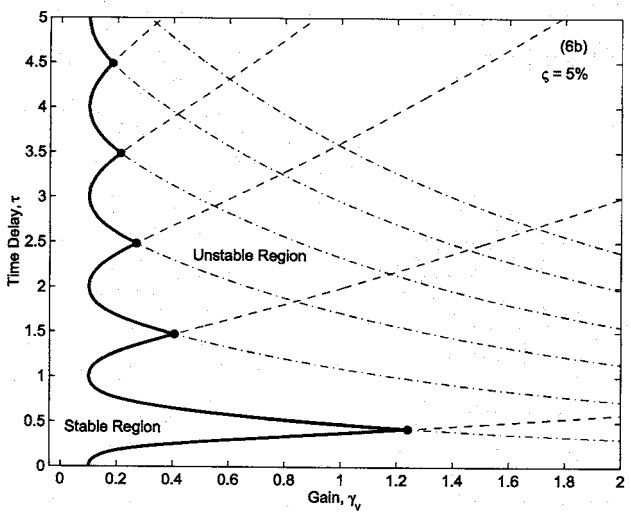

Fig. 6. Stability regions for: (a) $\zeta_n = 2\%$; and (b) $\zeta_n = 5\%$ using all poles of system with time-delayed PVF control

$$\gamma_v = -\frac{R^2 - 2\zeta_n R + 1}{R\exp(2\pi\tau R)} = -\frac{1 - (2\zeta_n - R)R}{R\exp(2\pi\tau R)} \tag{26}$$

Since $(2\zeta_n - R)R < 1$ for a real, positive value of R and $\zeta_n \ll 1$, $R^2 - 2\zeta_n R + 1$ is always positive. Also, $R\exp(-2\pi\tau R)$ is always positive for a real, positive value of R. Consequently, it is impossible that $\gamma_v > 0$. This shows that no poles exist along the negative real axis for PVF with time delays. Compared with the results given in Udwadia et al. (2005), we thus find that while we have a nonsystem pole with NVF for $\tau = 1$ coming up the real axis of the complex $\tilde{s}$ plane toward the origin as the negative feedback gain is gradually increased, no such nonsystem pole exists on the real axis with PVF for $\tau = 0.5$.

Besides dictating the maximum gain for stability, the nonsystem poles can interact with the system poles as the control gain increases. Let us consider the root loci of the nonsystem poles in the vicinity $\tau = 0.5$ as we gradually increase the positive feedback gain, γ_v. Up to a time delay $\tau < \tau_b \approx 0.5246$ [see Fig. 5(a)], as the gain is increased, the system pole and the nonsystem pole approach one another, and the nonsystem pole deflects upward while the system pole deflects downward past their region of encounter. In contrast, for $\tau > \tau_b$, beyond their region of encounter we see in Fig. 5(b) an apparent interchange of the "arms" between the two poles. This exchange of arms results in the root locus of the system pole deflecting upward as the gain increases, while that of the nonsystem pole deflects downward. Thus the behavior of the so-called system pole is intrinsically altered by its interaction with the nonsystem pole. A bifurcation occurs at $\tau = \tau_b$; for values of $\tau > \tau_b$ (respectively, $\tau < \tau_b$) the system pole moves upward (respectively, downwards) in the complex $\tilde{s}$ plane as the gain is increased. This explains the dramatic change in the qualitative behavior of the root loci (from "bending downward" to "bending upward") that was observed in Figs. 1(a–e) as the time delay is increased from $\tau = 0.5$ to 0.6.

Stability of Time Delayed Positive Velocity Feedback Control

The stability of the time delayed control for both positive feedback and negative feedback has been extensively studied in Udwadia et al. (2005) (see Fig. 11 in Udwadia et al. 2005) and so here we simply highlight some of the results that we will use in

the design of our positive velocity feedback control. We provide Fig. 6 so that it can be used as a design tool. Employing the results given in Udwadia et al. (2005), we see that the system with time delayed (for $\tau=0.5$) positive velocity feedback has a larger range of gains over which it is stable than that with time delayed (for $\tau=1$) negative velocity feedback. The maximum gain, γ_v, for stability for time delayed PVF with $\tau=0.5$ is 0.8557 for $\zeta_n=2\%$, and 0.8903 for $\zeta_n=5\%$ (see also Fig. 6). These values of the maximum gain for stability are virtually double those for time delayed NVF with $\tau=1$. We recall that these maximum gain values are dictated, as shown before, by the nonsystem poles, which cross over first into the right half complex plane, and not the system poles. Moreover, the maximum gain for stability in the vicinity of $\tau=0.5$ for positive velocity feedback is higher than that in the vicinity of $\tau=1$ for negative velocity feedback.

Applications

In this section we present two examples—one for a SDOF system and another for a multidegree of freedom (MDOF) structural system—of control design using positive velocity feedback and intentional time delays. Both systems are the same as those used in Udwadia et al. (2005), so that a detailed comparison between time-delayed PVF using an intentional time delay of half a period ($\tau=0.5$) can be made with time-delayed NVF with a time delay of a whole period ($\tau=1$). We show that not only is the PVF methodology proposed herein stable over a wider range of gains but it also shows improved performance and better control efficiency than the previously proposed (Udwadia et al. 2005) time-delayed NVF methodology.

Positive Velocity Feedback Control of SDOF System with Dimensionless Time Delay of $\tau=0.5$

Consider a SDOF system which has a damping factor $\zeta_n=2\%$ and a natural period $T_n=0.804$ s. It is subjected to the synthetically generated ground acceleration shown in Fig. 7(a). Our aim is to study the effectiveness of time delayed PVF with $\tau=0.5$ and compare it with time-delayed NVF with $\tau=1$. Using the results obtained in Fig. 2 we shall design the control gains so that the values of the equivalent damping factors are the highest in each case. We show these design gains in Table 1 for both PVF and NVF.

We note that the design gains are chosen so that the equivalent damping of the system poles is maximized in each case. However, the stability of the time-delayed control for both NVF and PVF, as pointed out in "Behavior of Nonsystem Poles," may not be controlled by these system poles but by the nonsystem poles. Hence it is necessary to determine whether the design gains chosen are not too large to make the system unstable. The last column in Table 1 gives the maximum gain for stability obtained from Fig. 6 for time-delayed PVF and from a similar figure for time-delayed NVF (see Fig. 11 in Udwadia et al. 2005). These figures result from a stability analysis that includes all the poles (system and nonsystem). Since our design gains are less than those at which the systems become unstable, our control design is guaranteed to be stable.

Fig. 7(b) shows 15 s of the large amplitude response of the system. The dashed line shows the uncontrolled response, and the dark solid line shows the controlled response using time-delayed PVF with $\tau=0.5$. The thin solid line shows the response using time-delayed NVF with $\tau=1$. As seen from the figure, our PVF control methodology has improved performance when compared to the previously proposed NVF methodology.

Fig. 7(c) shows the integral of the square of the responses (ISRs). We have shown the performance of the two types of control shown in Table 1. Comparing curves (2) and (5) it is seen that PVF with $\tau=0.5$ and $\gamma_v=0.31$ gives a better result than NVF with $\tau=1$ and $\gamma_v=0.124$. These gains are, respectively, the optimal gains, as shown in Fig. 2(a), for obtaining the largest equivalent damping factor from the root loci of the system poles of the time-delayed system. Fig. 7(c) also shows that both curves (2) and (5) are above curve (6), which is for direct velocity feedback with no time delay. However, comparing curves (0) and (5) we see that time-delayed PVF with $\tau=0.5$ and a gain of $\gamma_v=0.31$ provides a dramatic reduction in the ISR of the structural system.

To make a greater comparison we have also shown the performance of time delayed PVF (with $\tau=0.5$) when using the optimal gain for time-delayed NVF (with $\tau=1$) and vice versa. We observe, comparing curves (1) and (2) in Fig. 7(c), that when using NVF with the optimal gain corresponding to that of PVF (namely, the larger value, $\gamma_v=0.31$) the performance of the time-delayed NVF control is worse than with the optimal gain of $\gamma_v=0.124$. It is also interesting to compare curves (2) and (3). We observe that though the equivalent damping factor, as determined from Fig. 2(a) for time-delayed PVF is smaller than that for NVF when $\gamma_v=0.124$, the performance of PVF is still superior to that of NVF! This shows the important part that the nonsystem poles may play in reducing the quality of control performance as pointed out in "Behavior of Nonsystem Poles" (also see "Physics of Time-Delayed Velocity Feedback Structural Control" for a more physically based reason). From Fig. 3(a), we also observe a greater "softening" of the system with NVF compared to PVF at $\gamma_v=0.124$.

In Fig. 7(d) we show the integral of the square of the response (ISR) for velocity feedback control using three different control strategies as a function of the (absolute value of the) gain g_v. We compare direct velocity feedback with no time delay, NVF with a time delay $\tau=1$, and PVF with a time delay $\tau=0.5$. The ISRs are computed in each case over a duration of 40 s. As seen from the figure, for all values of gain shown in the plot, the PVF strategy leads to smaller responses (ISRs) than NVF, the superiority in performance of PVF over NVF gradually increasing with increasing gain.

Fig. 7(e) compares the integral of the square of the control force (ISC) for the same three velocity feedback control strategies described above. The ISCs are computed in each case over a duration of 40 s. We again see that time-delayed PVF with $\tau=0.5$ is superior in terms of control-force efficiency to time-delayed NVF with $\tau=1$, the superiority increasing with increasing gain values, over the range of gains shown.

In this example, as seen from Figs. 7(d and e), for a gain of 2, the control energy (ISC) required for time delayed NVF with $\tau=1$ is approximately 1.83 times that required for time-delayed PVF with $\tau=0.5$, while the ISR for time-delayed NVF with $\tau=1$ is about 1.77 times that for time-delayed PVF with $\tau=0.5$. We thus have greatly improved structural performance using time-delayed PVF with $\tau=0.5$ and far improved control efficiency when compared with time-delayed NVF with $\tau=1$. Finally, Figs. 7(d and e) also show that the performance and the control efficiency of time-delayed PVF may be acceptable even when compared with NVF with no time delay.

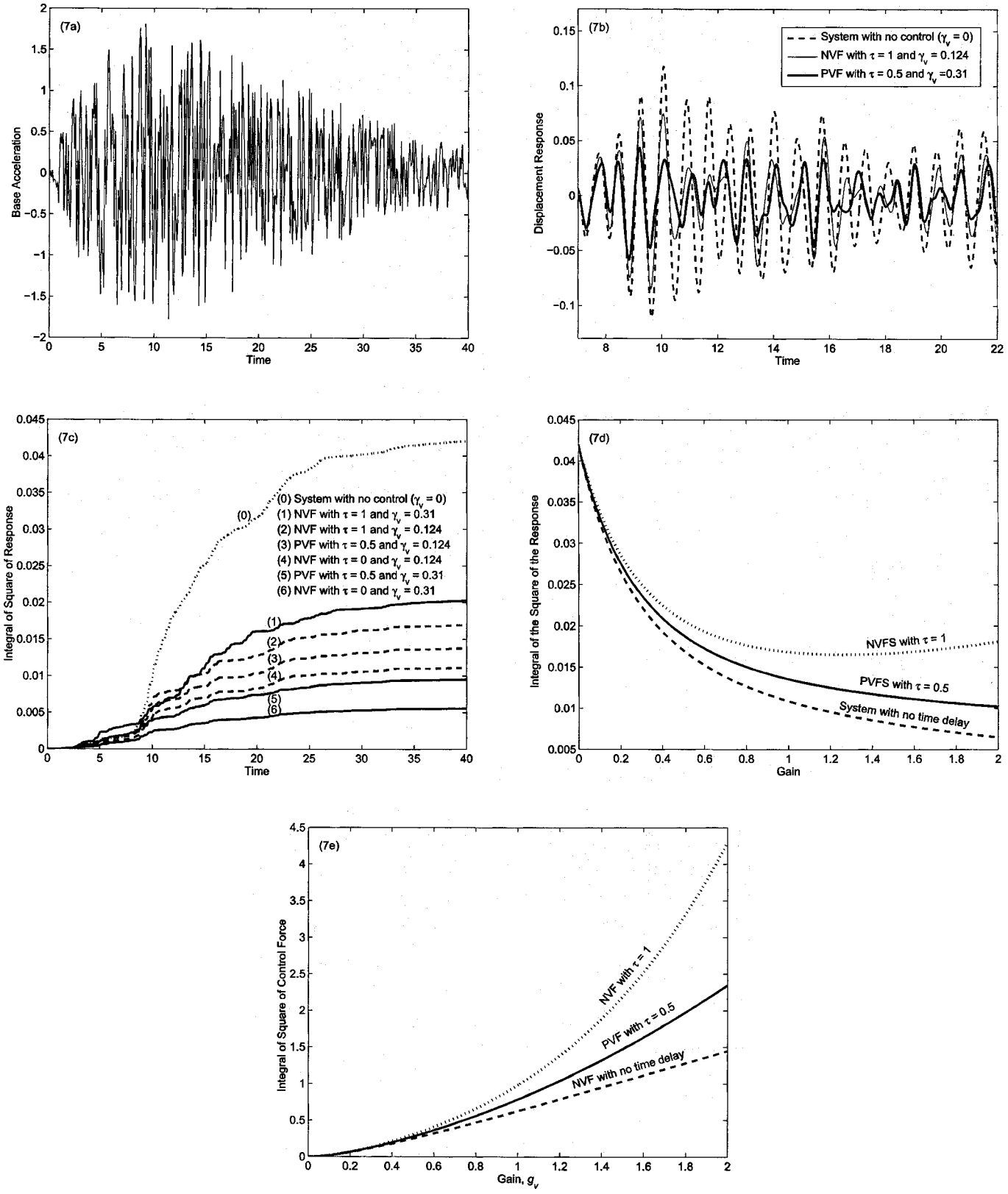

Fig. 7. (a) Synthetically computed base acceleration as function of time; (b) comparison of large amplitude response of SDOF system with different time-delayed velocity feedback control strategies and with no control; (c) comparison of integral of square of response (ISR) of SDOF system for various types of time-delayed velocity feedback control; (d) comparison of integral of square of response using time-delayed velocity feedback control as function of gain; and (e) comparison of integral of square of control force using time-delayed velocity feedback control as function of (absolute value of) gain

Table 1. Time Delays and Design Gains that are Used for Time Delayed PVF and NVF Control, and Maximum Gains over which Time-Delayed PVF and NVF are Stable

Types of feedback control	Time delay $T_d=\tau T_n$	Designed gain using Fig. 2 $\lvert\gamma_v^d\rvert(g_v=\omega_n\lvert\gamma_v^d\rvert)$	Maximum gain for stability using Fig. 6 $\lvert\gamma_v^{\max}\rvert(g_v=\omega_n\lvert\gamma_v^{\max}\rvert)$
PVF	0.402(τ=0.5)	0.31 (2.4226)	0.8557 (6.6872)
NVF	0.804(τ=1)	0.124 (0.97)	0.4737 (3.7019)

Noncollocated Distributed Control of MDOF Systems Using Time Delayed Positive Velocity Feedback

Let us consider a 3-DOF building structure with time delayed velocity feedback control

$$M\ddot{x} + C\dot{x} + Kx = f(t) + \sum_{i=1}^{i=3} G_i\dot{x}(t - T_{di}) \tag{27}$$

where M, C, and K=mass, damping, and stiffness matrices, respectively. The force vector $f(t)$ is taken in this example to correspond to a base acceleration caused by strong earthquake ground shaking. We take the S00E component of the El Centro earthquake of 1940 as our base acceleration. The last term of Eq. (27) represents the time-delayed velocity feedback control with the gain matrix G. Note that we use three different time delays, T_{di}.

We assume that the mass matrix of the structure is a 3×3 identity matrix and its stiffness matrix K is given by

$$K = \begin{bmatrix} 500 & -500 & 0 \\ -500 & 1{,}000 & -500 \\ 0 & -500 & 1{,}500 \end{bmatrix}$$

It is assumed that the system is classically damped so that each mode of vibration of the system can be decoupled separately. The damping matrix C is chosen in order to have the damping factors (ζ_n) for the three modes: 0.02 for the first mode; 0.05 for the second mode; and, 0.10 for the last mode.

By a suitable linear transformation, each modal response can be expressed in the form (see Udwadia et al. 2005)

$$\ddot{z}_i + 2\omega_{ni}\zeta_{ni}\dot{z}_i + \omega_{ni}^2 z_i = q_i(t) + g_i\dot{z}(t - T_{di}) \quad i = 1,2,3 \tag{28}$$

where the values of the damping factors (ζ_n) and the natural periods (T_n) corresponding to each mode are provided in Table 2.

We shall now demonstrate our time-delayed control design procedure on this MDOF system.

Since the third mode has a significant damping ratio, we shall control only the first two modes of the system. The gains that are used in each control feedback loop are designed from Fig. 2 such that the values of the equivalent damping factors corresponding to each mode are highest. The (absolute) values of the gains that we obtain for PVF and NVF are shown in Tables 3 and 4,

Table 2. Damping Factors and Natural Periods of Vibration for Each Mode of Uncontrolled Structural System

Modes	Damping factor (ζ_n)	Natural period $T_n=2\pi/\omega_n$ (s)
1	0.02	0.542836 (ω_n=11.5747395 rads/s)
2	0.05	0.198692 (ω_n=31.6227766 rads/s)
3	0.10	0.145452 (ω_n=43.1975162 rads/s)

Table 3. Time Delays and Design Gains That Are Used for Positive Velocity feedback (PVF) Control with Time Delay τ=0.5

Modes	Time delay $T_d=\tau T_n$	Design gain $\lvert\gamma_v^d\rvert$ using Fig. 2 $(g_v^d=\omega_n\lvert\gamma_v^d\rvert)$	Maximum gain for stability using Fig. 6 $\lvert\gamma_v^{\max}\rvert(g_v=\omega_n\lvert\gamma_v^{\max}\rvert)$
1	0.27	0.31 (3.5882)	0.8557 (9.9045)
2	0.10	0.29 (9.1706)	0.8903 (28.1538)

respectively. However, the stability of the system is controlled by nonsystem poles, as demonstrated in "Behavior of Nonsystem Poles." Thus, we have to consider the maximum gains so that the system is stable. We provide those values for PVF and NVF in Tables 3 and 4.

For convenience, we denote the set of design gains, $\gamma_v^d(g_v^d)$, for PVF with τ=0.5 as Gain Set 1 (GS1), and the set of gains designed for NVF with τ=1 as Gain Set 2 (GS2). When we refer to the values of the gains for NVF, we shall always mean their absolute values. After choosing the design gains, g_v^d, for each mode we can then suitably recombine them to provide the system gain matrices, G_i (for details, see Udwadia et al. 2005).

Figs. 8(a–c) show a comparison of the structural response during large amplitude motions using time delayed velocity feedback control shown in Tables 3 and 4. The base acceleration is the S00E component recorded in the El Centro, 1940, earthquake. As seen, there is a marked reduction in the response of the structural system; PVF control with time delay τ=0.5 gives us markedly smaller responses, especially peak responses, than NVF control with time delay τ=1.

Figs. 9(a–c) show a comparison of the control force required during the large amplitude response for the two different types of time-delayed velocity feedback control strategies. We observe that with PVF control with τ=0.5 we use substantially lower peak control forces than with NVF control with τ=1.

Figs. 10(a–c) show the integral of square of the response (ISR) for various types of time-delayed velocity feedback control as a function of time at each story level. Recall that the optimal "gain sets" for PVF and NVF are GS1 and GS2, respectively. These gain sets are determined by looking for the maximum damping factors given by the root loci of the "system poles" of the time-delayed system in each case. As we can see from curves (0), (2), and (5), there is a marked reduction in the response (ISR) of the structural system using both NVF and PVF time-delayed strategies. Furthermore, comparing curve (5) with curves (4) and (2), PVF with τ=0.5 and GS1 shows a much superior performance than NVF with τ=1 and GS2, or NVF with no time delay and GS2. However, NVF control with no time delay and GS1 is superior [compare curves (6) and (5)]. Also, as with our previous example, PVF with GS2 [curve (3)] is superior in performance to NVF with GS2 [curve (2)], again showing that the nonsystem poles may play a very significant part in the structural response.

Table 4. Time Delays and Design Gains that are Used for NVF Control with Time Delay τ=1

Modes	Time delay $T_d=\tau T_n$	Design gain $\lvert\gamma_v^d\rvert$ using Fig. 2 $(g_v^d=-\omega_n\lvert\gamma_v^d\rvert)$	Maximum gain for stability using Fig. 6 $\lvert\gamma_v^{\max}\rvert(g_v=-\omega_n\lvert\gamma_v^{\max}\rvert)$
1	0.54	0.124(−1.4353)	0.4737(−5.4830)
2	0.20	0.106(−3.3520)	0.5108(−16.1529)

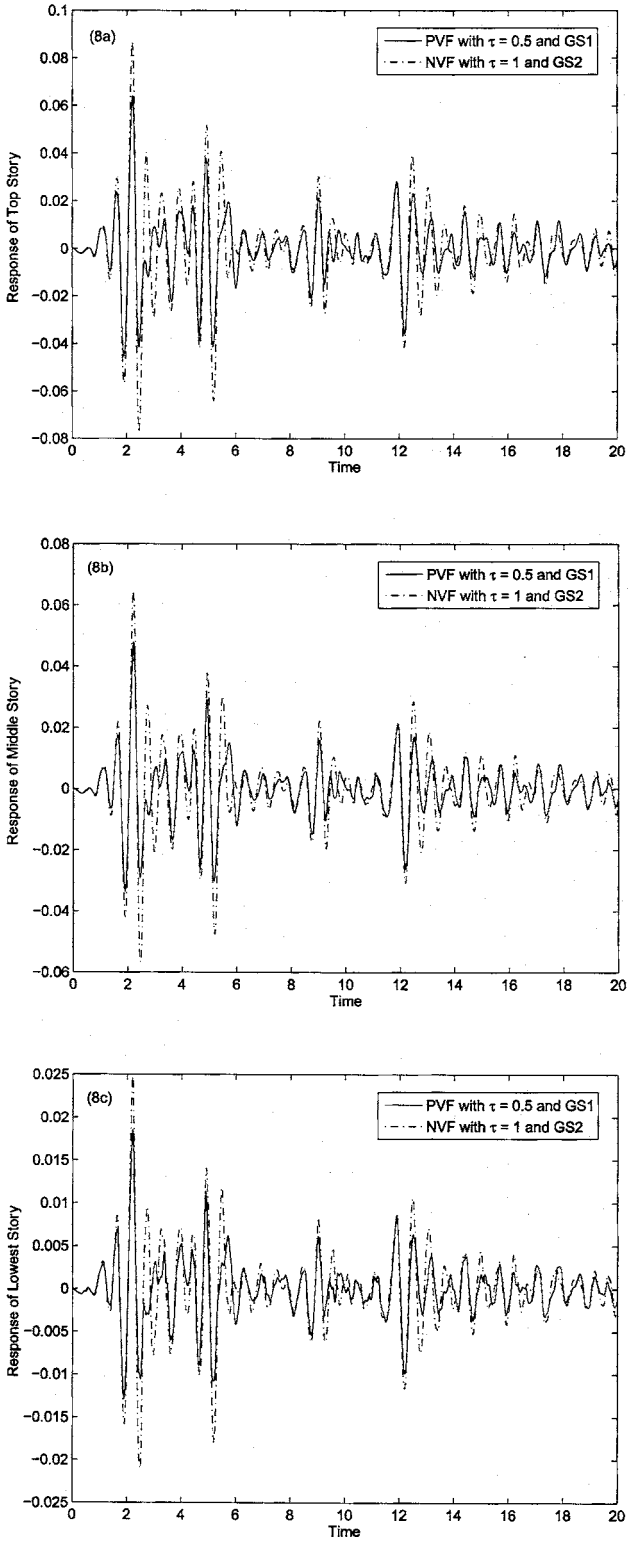

Fig. 8. Comparison of response of three-storey structure during large amplitude response as function of time using different time-delayed velocity feedback methodologies (PVF with $\tau=0.5$ and NVF with $\tau=1$)

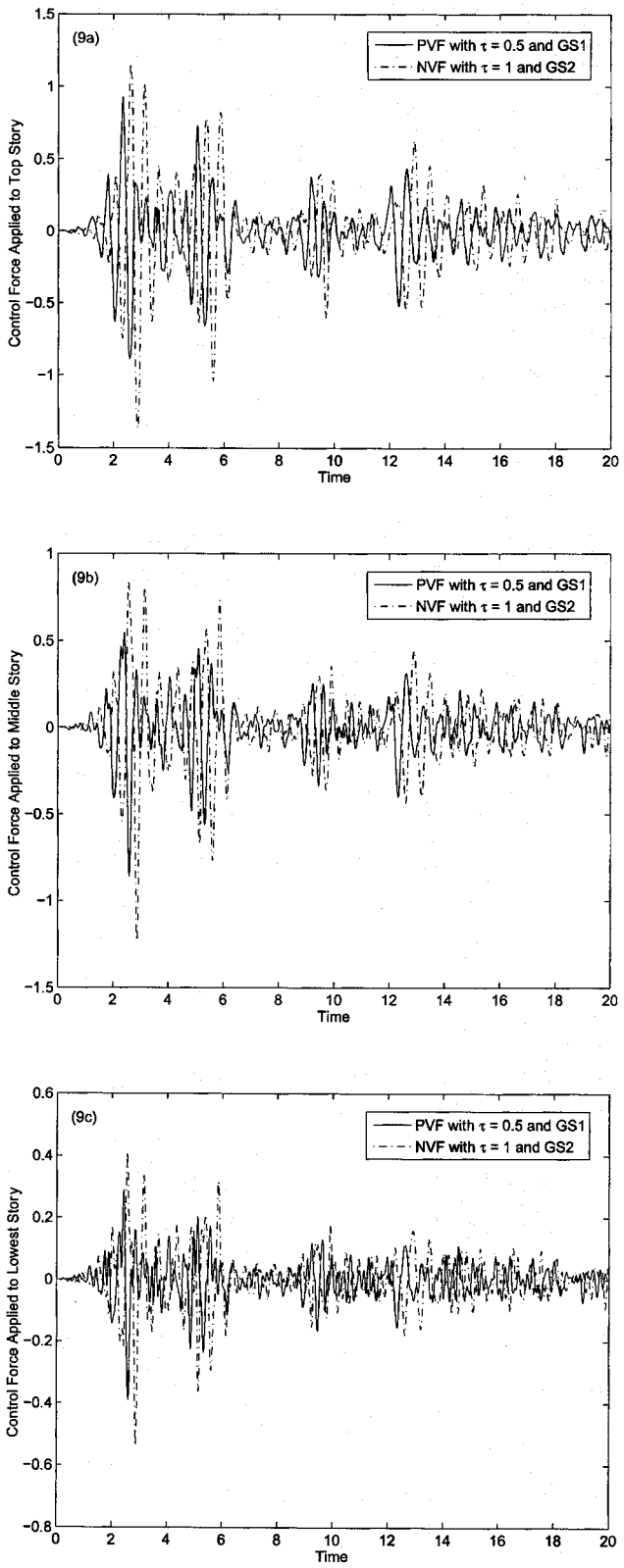

Fig. 9. Comparison of control force required during large amplitude response for PVF with $\tau=0.5$ and NVF with $\tau=1$ as function of time

Figures 11(a–c) show the integral of the square of the control force (ISC) for various types of time-delayed velocity feedback control as a function of time at each of the story levels. While NVF with no time delay using GS1 is the most cost efficient control [curve (6)], we see that PVF with $\tau=0.5$ and GS1 is also quite efficient [curve (5)]. As shown, PVF with $\tau=0.5$ and GS1 [curve (5)] is more control-energy efficient than NVF with $\tau=1$ whether using GS1 or GS2 [see, curves (1) and (2)], and NVF with no time delay with GS2 [curve (4)]. Furthermore, PVF with $\tau=0.5$ [curve (3)] even with GS2 is more efficient than NVF with GS2, or with GS1 [curves (1) and (2)].

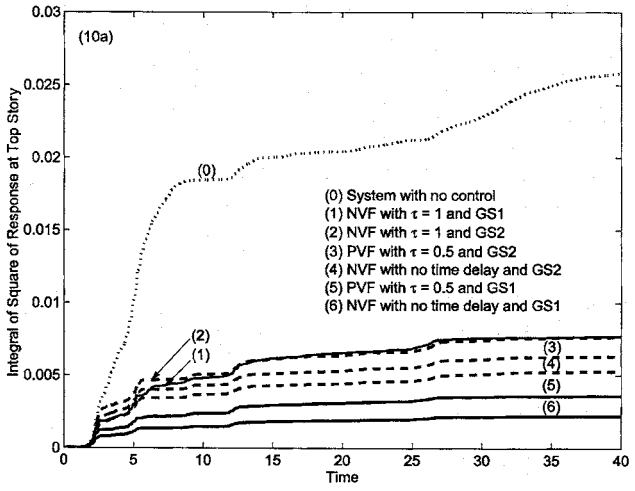

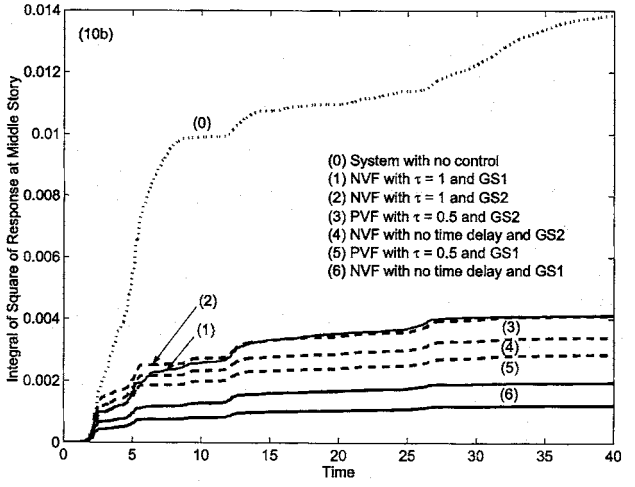

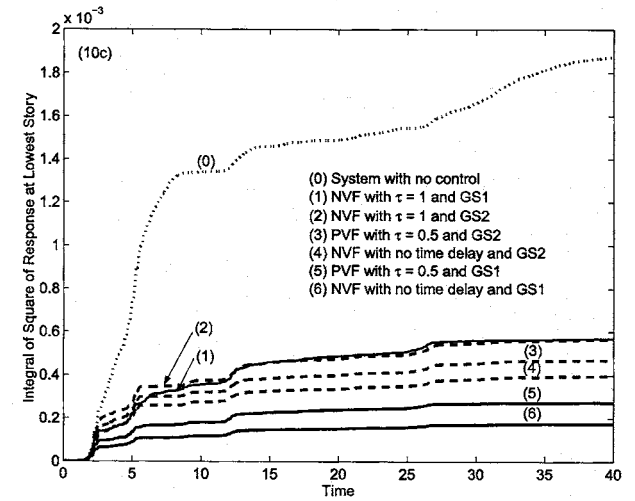

Fig. 10. Comparison of integral of square of response as function of time for various types of time-delayed control for MDOF system

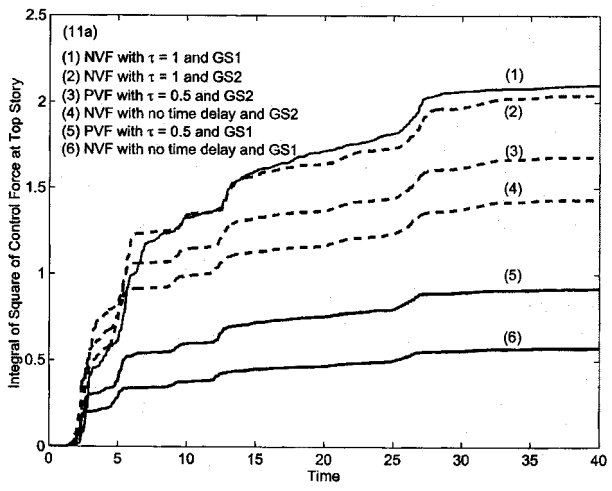

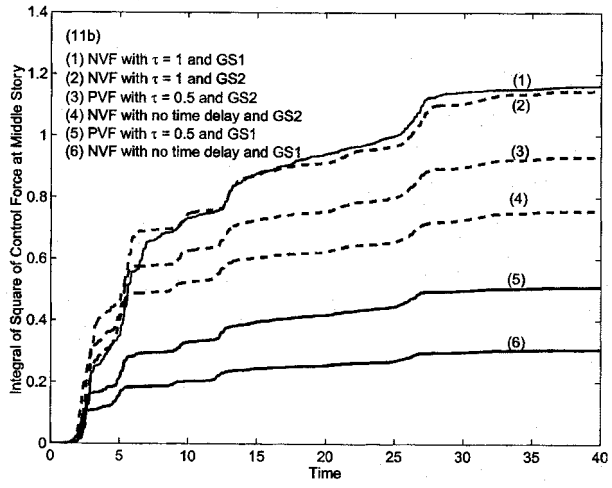

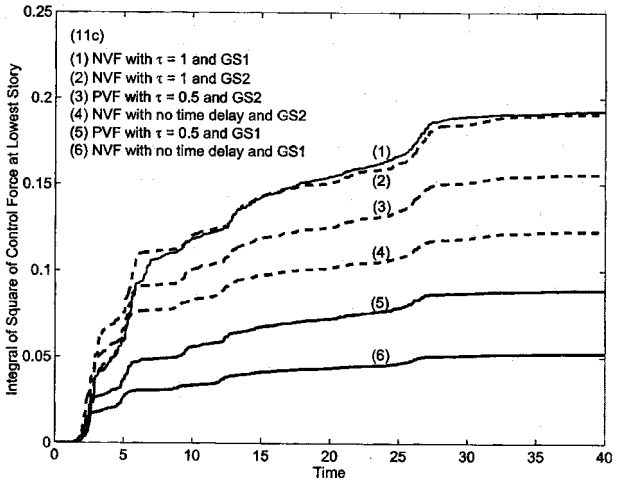

Fig. 11. Comparison of integral of square of control force required (as function of time) for various types of time-delayed velocity feedback control

From Figs. 10 and 11 we see that NVF performance for this MDOF system is generally about the same [curves (1) and (2), Fig. 10] when GS1 is used instead of GS2, and so is the control efficiency [curves (1) and (2), Fig. 11], though in the region of large amplitude responses GS2 appears slightly superior to GS1. Also, from the curves in these figures we see that time-delayed PVF with GS1 gives both the best performance and the best control efficiency [curves (5) in Figs. 10 and 11], and in both performance and control efficiency it is fairly comparable to that achieved with negative velocity feedback with no time delays [curves (6) in Figs. 10 and 11]. This demonstrates the apparent

superiority of our PVF control design (with $\tau=0.5$ and GS1) over time-delayed NVF both in terms of performance and control efficiency.

Physics of Time-Delayed Velocity Feedback Structural Control

In this section, we attempt to understand more of the physics of velocity feedback control with time delays. The basic problem that arises in structural control is that time delays may creep into the control loop primarily because of delays in sensing the motions, in control force computations, and in the application of the active control forces, which are generally large and are often required at high frequencies. Were such time delays to be absent negative velocity feedback, which essentially increases the equivalent damping in the system, would be an efficient and simple way of performing structural control. We note that in using direct velocity feedback one uses information about the instantaneous velocity of the system in the feedback loop.

We have shown in this paper that when such instantaneous information cannot be employed during feedback due to inherent time delays, positive velocity feedback (PVF) with a time delay $\tau=0.5$, and negative velocity feedback (NVF) with a time delay of $\tau=1$ (see Udwadia et al. 2005) could be used, the former being generally superior. We have shown that time-delayed PVF control design, though somewhat inferior compares well, both in performance and in control efficiency, with direct velocity feedback control (with no time delay).

To understand the physical reason for this, consider first a system whose response is completely sinusoidal. Shifting the response signal, or the velocity signal, forward or backward by exactly one period then leaves the signal invariant. Hence if negative velocity feedback with no time delay is effective, then negative velocity feedback with a time delay of an entire period (or its multiple) would likewise also be equally effective. Similarly, shifting a sinusoidal response, or the velocity signal, by half a period and "flipping" it will again leave it invariant and that is why if negative velocity feedback with no time delay is effective, then using a positive velocity feedback—we flip the sign of the gain instead, because we cannot flip the signal!—with a time delay of half a period would also be equally effective.

However, the response and velocity of the system are generally not truly sinusoidal. The velocity signal is composed of several sinusoids having different phases and amplitudes. Therefore shifting the signals in the ways mentioned above would really not leave things invariant. The more nearly we use the instantaneous velocity information with no time delay, as is done in direct velocity feedback, the closer our time delayed control will be in its effectiveness to it. In general, the more we shift from instantaneous control, the more likely we are to have changes in the signal. This is why PVF control with $\tau=0.5$, where we shift the velocity signal by only half a period, is superior to NVF control with $\tau=1$ where we shift it by a whole period.

While the above physical explanation is heuristic at best, it is reflected in several (and more exact) analytical counterparts, which is why PVF control with $\tau=0.5$ appears to be superior to NVF control with $\tau=1$. The analytical results indicate that: (1) The maximum equivalent damping factor attainable with PVF appears to be greater than that attainable with NVF (see Fig. 2). (2) The nonsystem poles are farther apart for PVF since the time delay used is half of that used with NVF [see Eq. (23)], and hence, in general, their effect on the system's response is reduced: lesser higher frequency effects caused by the presence of nonsystem poles and diminished interference with the system poles. (3) The maximum gains for stability are also roughly doubled for the nonsystem poles again because the time delay used with PVF is half of that for NVF [see Eq. (24)], making PVF stable over a larger range of control gains. (4) PVF has no poles on the real axis to affect the system's response as does NVF.

Conclusions

In this paper we present a new methodology for controlling structural system using time-delayed positive velocity feedback control. We expand the principles that are given by Udwadia et al. (2005), which mainly dealt with negative velocity feedback control, to time delayed positive velocity feedback control. Our study considers performance, stability, and control efficiency of such control systems, which are shown to be basically dominated by system and nonsystem poles.

By considering the behavior of the system poles of a SDOF system with positive velocity feedback control, it is shown that the equivalent damping factor is high when using intentional time delays in the vicinity of half the natural period of vibration of the system ($\tau\approx0.5$). Also, it is found that over a certain range of feedback gains equivalent damping factors are higher compared with using negative velocity feedback with $\tau=1$ or with no time delay. As a result, we explore a design strategy that uses a time delay $\tau\approx0.5$ and an appropriate design gain so that the value of the equivalent damping factor is highest.

However, the system is actually infinite dimensional, and it has an infinity of poles that do not start from the system poles when $\tau=0^+$. We show that performance and stability of the time-delayed system in fact may not be controlled by the system poles, but by the nonsystem poles. Therefore, we further investigate the behavior of these nonsystem poles and our study shows that time-delayed positive velocity feedback control, in general, reduces the effect of the nonsystem poles on the system poles, and on the response of the system to external excitations when compared with time-delayed negative velocity feedback. This is because there is a greater spacing between the root loci of the nonsystem poles. More than that, the stream of roots on the negative real axis occurring when using negative velocity feedback control disappears when using positive velocity feedback control. The stability regions obtained herein show that time-delayed positive velocity feedback control with $\tau\approx0.5$ is stable over a wider range of control gains than is time-delayed negative velocity feedback control with $\tau\approx1$.

The lower interaction between the nonsystem and system poles causes our design strategy that uses time-delayed positive velocity feedback control with $\tau\approx0.5$ to have not just improved performance and stability characteristics, but also leads to much improved control-force efficiency. Thus our design shows marked improvements over previously proposed time-delayed negative velocity feedback control designs (Udwadia et al. 2005).

Finally, we demonstrate through numerical examples the efficacy of our control design applied to both SDOF and MDOF vibratory structural systems. We use a synthetic accelerogram and study the response of a SDOF system; and we use the S00E acceleration component of the El Centro, 1940, earthquake as the base acceleration to a three story structure. The computational results validate our expectations. We illustrate that the proposed time-delayed control design is amply stable; it has markedly superior performance when compared to the negative velocity

feedback (with $\tau \approx 1$) that was proposed earlier (Udwadia et al. 2005). In the range of gains studied, it has fairly comparable, though slightly inferior, performance and control-efficiency characteristics when compared with standard negative velocity feedback with no time delay.

The control design proposed herein would therefore be useful for mitigating structural damage caused by external forces such as those induced by strong earthquake ground shaking and strong winds. The introduction of intentional time delays in control loops is usually a simple matter to implement, and hence the design proposed in this paper shows promise from a practical, real-life standpoint. However, the fact that relatively large time delays do occur in structural systems and that they could be used to advantage in structural control is an area of research that has only recently emerged, and a lot still remains to be done.

References

Abdel-Rohman, M. (1985). "Structural control considering time delay effect." *Trans. Can. Soc. Mech. Eng.*, 9, 224–227.

Abdel-Rohman, M. (1987). "Time-delay effects on actively damped structures." *J. Eng. Mech.*, 113, 1709–1719.

Agrawal, A. K., Fujino, Y., and Bhartia, B. (1993). "Instability due to time delay and its compensation in active control of structures." *Earthquake Eng. Struct. Dyn.*, 22, 211–224.

Agrawal, A. K., and Yang, J. N. (1997). "Effect of fixed time delay on stability and performance of actively controlled civil engineering structures." *Earthquake Eng. Struct. Dyn.*, 26, 1169–1185.

Agrawal, A. K., and Yang, J. N. (2000). "Compensation of time-delay for control of civil engineering structures." *Earthquake Eng. Struct. Dyn.*, 29, 37–62.

Choksy, N. H. (1962). "Time lag systems." *Prog. Control Eng.*, 1, 17–38.

Kobori, T., Koshika, N., Yamada, Y., and Ikeda, Y. (1991). "Seismic-response-controlled structure with active mass driver system, Part 1: Design." *Earthquake Eng. Struct. Dyn.*, 20, 133–149.

Koike, Y., Murata, T., Tanida, K., Mutaguchi, M., Kobori, T., Ishii, K., Takenaka, Y., and Arita, T. (1994). "Development of v-shaped hybrid mass damper and its application to high-rise buildings." *Proc., 1st World Conf. on Structural Control*, University of Southern California Press, Los Angeles, Calif., FA2-3–FA2-12.

Marshall, J. E. (1974). "Extensions of O. J. Smith's method to digital and other systems." *Int. J. Control*, 19, 933–939.

Sain, P. M., Spencer, B. F., Jr., Sain, M. K., and Suhardjo, J. (1992). "Structural control design in the presence of time delays." *Proc., 9th Engineering Mechanics Conf.*, ASCE, New York, 812–815.

Satche, M. (1949). "Stability of linear oscillating systems with constant time lag." *J. Appl. Mech.*, 16, 419–420.

Udwadia, F. E. (1991). "Noncollocated point control of nondispersive distributed-parameter systems using time delays." *Appl. Math. Comput.*, 42(1), 23–63.

Udwadia, F. E. (1992). "Noncollocated time delayed control of continuous systems with tip-inertias." *Appl. Math. Comput.*, 47, 47–75.

Udwadia, F. E., and Kumar, R. (1994a). "Time delayed control of classically damped structural systems." *Int. J. Control*, 60, 687–713.

Udwadia, F. E., and Kumar, R. (1994b). "Time delayed control of classically damped structures." *Proc., 11th World Conf. on Earthquake Engineering*, Acapulco, Mexico.

Udwadia, F. E., von Bremen, H., Kumar, R., and Hosseini, M. (2003). "Time delayed control of structures." *Earthquake Eng. Struct. Dyn.*, 32, 495–535.

Udwadia, F. E., von Bremen, H., and Phohomsiri, P. (2005). "Time delayed control design for active control of structures: Principles and application." *Structural Control Health Monitoring*, 12(3).

von Bremen, H., and Udwadia, F. E. (2000). "Can time delays be useful in the control of structural systems?" *Proc., 42nd AIAA/ASME/ASCE/AHS Structures, Dynamics and Materials Conf.*, Atlanta.

von Bremen, H., and Udwadia, F. E. (2001). "Effect of time delay on the control of a torsional bar." *Proc., 43rd AIAA/ASME/ASCE/AHS Structures, Dynamics and Materials Conf.*, Seattle.